

Gaseous Inhibitors: A Comprehensive Overview on Mitigating Hydrogen Embrittlement in Pipeline Steels

Jubica^a, Lisa Claeys^a, Aurélie Laureys^a, Wim De Waele^b, Julien Schweicher^c, Tom Depover^a, Kim Verbeken^a

^a*Ghent University, Department of Materials, Textiles and Chemical Engineering, Research group of Sustainable Materials Science, Technologiepark 46, Zwijnaarde, 9052, Belgium*

^b*Ghent University, Department of Electromechanical, Systems and Metal Engineering, Soete Laboratory, Technologiepark 46, Zwijnaarde, 9052, Belgium*

^c*Fluxys, Kunstlaan 31, Brussels, 1040, Brussels, Belgium*

Abstract

Hydrogen transport via new and existing natural gas pipelines is promising in the shift to more renewable energy as an efficient energy carrier is of utmost importance due to the discrepancy in timing between production and use of the energy. However, the risk of hydrogen embrittlement (HE) in pipeline steels exposed to pure hydrogen gas poses a significant challenge. An emerging approach to this issue involves adding trace amounts of inhibitor gases to the hydrogen gas such as oxygen or carbon monoxide. This work provides a comprehensive overview of the mitigation of HE in pipeline steels using these gaseous additives. While there is limited literature on the hydrogen/surface interaction with pipeline steels, numerous studies focus on the surface science of individual gaseous additives on clean iron surfaces. This overview delves deeper into the surface chemistry of these inhibitor gases when exposed to clean iron surfaces, emphasizing the competitive interactions of these gases in the presence of pure hydrogen. Introducing gaseous inhibitors in pure hydrogen reduces hydrogen absorption by slowing down the adsorption kinetics of hydrogen gas. However, during longer exposure times, the presence of inhibitors does not prevent hydrogen from reaching an equilibrium condition. Hence, a continuous supply of these inhibitors is essential for sustained mitigation. Moreover, various factors, including the type of mechanical test, hydrogen pressure, and inhibitor gas concentration influence the effectiveness of the HE mitigation by gaseous inhibitors. A clear overview on these parameter influences for pipeline steels is given in this work.

Preprint submitted to International Journal of Hydrogen Energy

July 26, 2024

Keywords: Gaseous inhibitors, Hydrogen embrittlement, Pipeline steels

1. Introduction

Climate change urges us to align with the global goal of carbon neutrality. In this regard, the European Union (EU) commits to an economy with net-zero greenhouse gas emissions by 2050. This goal is central within the European Green Deal[1] and aligns with EU's commitment to global climate action under the Paris Agreement [2]. Hence, it is necessary to transition from non-renewable fossil fuels to sustainable alternatives. While active research is ongoing for renewable resources, there is a significant need for alternate green energy carriers that can smoothly complement fossil fuels. Hydrogen emerges as a promising candidate in this pursuit, promising to serve as a versatile and impactful energy carrier. The European Hydrogen Backbone (EHB) initiative seeks to accelerate Europe's transition to a low-carbon future by highlighting the crucial role of hydrogen infrastructure and utilizing existing and new pipelines [3].

Establishing a new pipeline network requires a substantial upfront investment and time. Mid-strength pipeline steels, such as API 5L grades X42, X46, and X52, have been employed for hydrogen transport. These pipelines can operate at pressures reaching up to 13 MPa [4, 5]. Swiftly transitioning to a sustainable energy economy will, therefore, involve leveraging existing natural gas infrastructure for hydrogen transport. However, repurposing natural gas pipeline steels for hydrogen transport has numerous complexities. Most high-pressure oil and gas pipelines consist mainly of body-centred cubic (BCC) phases, for example, polygonal ferrite, martensite (BCT) or bainite, which play a role in the embrittlement because of its low hydrogen solubility and high hydrogen diffusivity [6, 7]. Pearlite is also prone to hydrogen damage at the interfaces of ferrite and cementite where hydrogen is trapped [8]. Additionally, M/A constituents and retained austenite (RA) impact the sensitivity to hydrogen embrittlement [9]. RA having low hydrogen diffusivity and high solubility poses a particular risk if it transforms into martensite [10, 11]. This phenomenon is known as Hydrogen Embrittlement (HE). Hydrogen not only favours subcritical cracking and increases the fatigue crack growth rate (FCGR) but also reduces the ductility and fracture toughness of pipeline steels, as studied in [6, 7, 12, 13]. Substituting natural gas with hydrogen in existing high-pressure pipeline systems could accelerate the deterioration of mechanical properties [13]. It

is essential to account for structural variations in pipelines, such as bends, cracks, or weld defects, as they can exacerbate the interaction between hydrogen and materials. Additionally, the common use of impressed current cathodic protection to prevent steel corrosion introduces a potential challenge of inadvertently allowing atomic hydrogen to permeate the material's microstructure. Even though this process is relatively well controlled, it leads to a loss of structural and mechanical integrity [14, 15]. During the hydrogen transport, however, multiple potential hydrogen sources will exist: internal (generated during material production) and external (generated during service, corrosion and corrosion protection and gaseous hydrogen transport within the pipeline), all contributing to the overall degradation of the mechanical properties [16].

This work focuses on the gaseous hydrogen adsorption at the inner iron (Fe) surface, which is a gas-molecule competition. While HE occurs in the subsurface and bulk of the material, gas-molecule competition on the Fe surface determines the actual hydrogen concentration absorbed into Fe. Thus, common mitigation strategies include methods to control hydrogen-material surface interactions. Strategies like coatings and permeation barriers have been extensively reviewed in [17, 18, 19, 20], while material modifications were reported in [19, 20, 21, 22]. Another HE mitigation strategy involves introducing gas impurities into the hydrogen gas. Given the current lack of a comprehensive literature overview on gaseous inhibitors, this paper provides a detailed understanding of the role played by potential inhibitors in limiting HE in pipeline steels. The next sections will focus on the mechanism of gaseous hydrogen adsorption and absorption, the competition with gaseous inhibitors on the iron surface and finally, the mechanical validation of the HE mitigation effect, including an overview of various test parameter influences.

2. Mechanisms of hydrogen entry

The interaction between gases and solids involves three main steps: physisorption, chemisorption, and absorption [19, 23, 24]:

- Physisorption is a type of adsorption where a gas or liquid is attracted to a solid surface due to weak van der Waals forces. This attraction leads to the formation of a multilayer fluid which is reversible. The process occurs quickly, often happening instantaneously, and results

in a thin layer of adsorbate on the surface of the solid. The enthalpy change is roughly equivalent to the heat of condensation of the gaseous adsorbent, which is generally low. This suggests that during physisorption, as gas molecules adhere to the surface of the solid material, the enthalpy change is similar to the energy released when the gas condenses into a liquid [23].

- Chemisorption is a chemical process where a reaction between surface atoms and adsorbent molecules occurs. This process is limited to a monolayer, due to the short-range chemical forces at play. The process of chemisorption is activated and gradual, with possible irreversibility. This process involves the creation of a polarized, one-centre covalent bond between the surface atoms and the adsorbent, which results in a change in enthalpy known as the heat of adsorption. For instance, the heat of adsorption associated with the dissociative chemisorption of hydrogen on transition metals is related to the bond energies of MH and H-H pairs. Chemisorption is a slow, activated process, either slowly reversible or irreversible [23].
- The third and final step of the process is absorption, which entails incorporating the chemisorbed products into the metal's bulk lattice. The final absorption step in iron at room temperature is likely the slowest for gaseous hydrogen entry. Hydrogen absorbed in steel can later escape through the reverse of these three steps, highlighting a reversible process [24].

2.1. Catalytic dissociation of hydrogen

For an H₂ molecule to absorb onto the surface, it must undergo a chemical bonding process. The electron density between the hydrogen molecule and the Fe surface increases as it approaches the surface, Figure 1a. This suggests a bonding interaction between the d-orbitals of Fe and the antibonding σ^* orbital of the H₂ molecule. Such a bonding relationship provides evidence for surface-molecule electron transfer, which results in electron occupation of the antibonding σ^* orbital of the H₂ molecule. The σ^* orbital is distinguished by the presence of a nodal plane between the two H nuclei and its partial occupation causes instability and breaking of the H-H bond. Thus, hydrogen dissociation is catalysed by

electron transport from the Fe surface to the σ^* antibonding molecular orbital of the hydrogen molecule, Figure 1b [25].

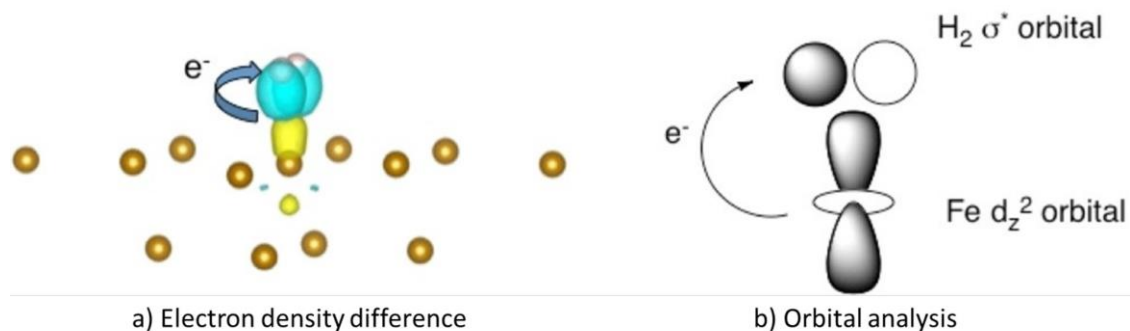


Figure 1: H₂ activation at the Fe surface. The electron density is transferred from the d_z^2 Atomic Orbital to the σ^* Molecular Orbital of H₂ molecule. e^- is the electron density shift. (a) Difference in electron density, where golden spheres are Fe atoms, white spheres are H atoms, blue colour indicates positive electron density, while yellow colour indicates negative electron density; (b) schematic orbital analysis. Reproduced from [26].

2.2. Iron-hydrogen interaction: surface dynamics and preferred sites

The iron-hydrogen interaction depends on the type of crystallographic plane that is available. Figure 2 shows the different sites in Fe(100), Fe(110) and Fe(111), respectively. The (100) plane has top (T), bridge (B), and 4-fold hollow (4F) sites; (110) has top (T), short-bridge (SB), long-bridge (LB), and 3-fold (3F) sites; (111) has top (T), shallow-hollow (SH), deep-hollow (DH), and 4-fold hollow (4F) sites. The atomic density values are in the order of (110) > (100) > (111). The electron-donating capacity of the Fe surface increases as the atomic density on the surface increases. For the following sections on hydrogen surface dynamics and hydrogen preferred sites, only the Fe(100) plane will be discussed.

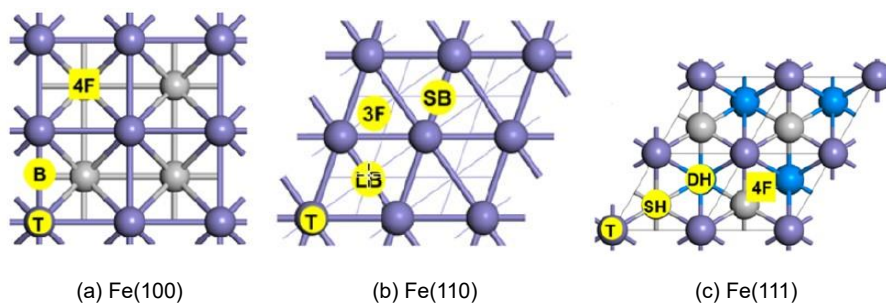


Figure 2: Schematic top views of (a) Fe(100), (b) Fe(110), and (c) Fe(111) with possible adsorption sites. (T) top site, (B) bridge site, (4F) 4-fold hollow site, (SB) short-bridge site (SB), (LB) long-bridge site, (3F) 3-fold site, (SH) shallow-hollow site, (DH) deep-hollow site. Reproduced from [27].

2.2.1. Hydrogen surface dynamics

The Fe surface offers adsorption sites for the hydrogen dissociation reaction, the rate of which is proportional to the concentration of hydrogen atoms in the bulk [25]. The energy landscape for hydrogen at the surface, sub-surface, and bulk of Fe(100) plays a pivotal role in determining the subsequent absorption of hydrogen. In the sub-surface of Fe, endothermicity between reaction steps poses a challenge for hydrogen absorption. However, the low packing density on Fe(100) and the limited hydrogen solubility in body-centred cubic (bcc) Fe facilitate hydrogen diffusion into the sub-surface, enhancing hydrogen mobility [28]. In contrast, the egress of hydrogen from iron is relatively straightforward, as the energy barrier for exit is lower than the ingress process.

2.2.2. Hydrogen preferred sites

Density Functional Theory (DFT) simulations were done in [26, 28] to explore hydrogen molecule interactions with a clean Fe(100) surface. A bcc iron model system was chosen as the literature suggests that the acceleration of fatigue crack growth in ferrite-pearlite steels stems mainly from hydrogen induced fatigue crack growth in the ferrite component, modelled here by bcc iron, [26]. Staykov et al. [26] highlighted the significance of H₂ molecule orientation with respect to the surface and the initial adsorption site of the surface for the H-H bond cleavage to occur. Cleavage occurs through electron transfer from the surface to the σ^* orbital of the H₂ molecule, demanding a favourable spatial orientation and a short surface-molecule distance. Optimal overlap is attained when H₂ is adsorbed on the top of a Fe atom in a side-on orientation. Conversely, bridge-site orientations lack the observed chemisorption state. The activated migration of hydrogen atoms that makes surface sites available for further adsorption is the rate-determining step in the adsorption process. Additionally, the activation energy for migration is a function of the fraction of surface covered [29]. In contrast, Jiang et al. [28] demonstrated that the 4-fold hollow site is the preferred location for hydrogen at Fe (100). The dissimilarity in findings may be associated with variations in the DFT

simulation methodologies employed. However, a detailed discussion on DFT methods lies outside the scope of this paper. In summary, the adsorption of hydrogen on the Fe(100) plane is influenced by the orientation of the hydrogen molecule relative to the surface and the energy landscape within the Fe/H system.

2.3. Sievert's law

The unique feature of the H/Fe system is rooted in the minimal lattice parameter of bcc Fe. This characteristic pertains to the small interstitial space and the close nearest-neighbour interstitial distances, creating a scenario where H exhibits low solubility within the bcc Fe lattice and high mobility. As a result, hydrogen swiftly moves towards surfaces or finds its way to trapping sites such as crack tips, vacancies, grain boundaries, or alloying elements after its absorption into the iron lattice, leading to HE [28]. Sievert's law is a fundamental concept that explains how gases absorb in metals. This law states the relationship between the amount of gas absorbed in a metal and the partial pressure of that gas in its environment. For hydrogen absorption conditions under equilibrium, hydrogen solubility (C_H) in steels is given by the expression, [30]:

$$C_H = K\sqrt{p_{H_2}}$$

where K is the temperature-dependent equilibrium coefficient, and p_{H_2} is the hydrogen partial pressure. This expression characterizes the equilibrium hydrogen content in steels under high-temperature or low-partial-pressure conditions.

At high pressures and low temperatures, the behaviour of hydrogen gas becomes critical as it deviates from ideal gas behaviour. In such cases, it is important to substitute p_{H_2} with fugacity f , [31, 32]. Thus, the equation becomes

$$C_H = S\sqrt{f_{H_2}}$$

where C_H is the amount of hydrogen dissolved in the steel, S is the Sievert's constant or solubility constant, and f_{H_2} is the hydrogen fugacity at the steel surface.

Using the Abel-Noble equation of state, the hydrogen fugacity can be calculated from the partial pressure of hydrogen, as given below:

$$f_{H_2} = p_{H_2} \exp\left(\frac{p_{H_2}b}{RT}\right)$$

where p_{H_2} is the partial pressure of hydrogen, b denotes a constant ($1.584 \times 10^{-5} \text{ m}^3 \text{ mol}^{-1}$), T denotes the temperature in K, and R denotes the gas constant ($8.314 \text{ JK}^{-1} \text{ mol}^{-1}$) [33, 34].

2.4. The interaction with active deformation

Adsorption of hydrogen during HE testing is eased by surface deformation. High dislocation densities produced near a crack tip, for example, provide catalytically more active surface sites as these structural irregularities in the crystal lattice are characterised by regions of high strain and increased atomic disorder. Lattice dilatation (or expansion) and contraction occurs near a dislocation. Strain also leads to an abrupt change in the electron distribution near a dislocation. To maintain a constant Fermi surface throughout the crystal, conduction electrons undergo a redistribution in response to the strain caused by the dislocation. The charge redistribution results in the formation of an electric dipole on the dislocation line. The electric field generated by the dislocation-induced charge redistribution is restricted and its influence is localized in the immediate vicinity of the dislocation core. Thus, dislocations are sites of high localised energies [35].

High surface energy sites provided by dislocation intersections with the surface lead to a higher hydrogen dissociation rate and thus more rapid crack growth [36, 37]. Studies conducted by Xu et al. [38, 39] on how tensile stresses affect hydrogen adsorption and permeation in X70 pipeline steel suggested that applied tensile stress increased the surface energy [38]. This increase enhanced the hydrogen dissociation rate by reducing adsorption energy and increasing desorption energy on the surface [39]. The concentration of hydrogen in the sub-surface increased as the applied stress intensified. Thus, stress fields must be taken into account while evaluating for hydrogen solubility. A more parameterized form of Sievert's law is given by the expression, [40]:

$$C_{\text{H}} = K \sqrt{f_{\text{H}_2}} \exp\left(\frac{V_{\text{H}} \sigma_{\text{H}}}{RT}\right)$$

where f_{H_2} is the fugacity of hydrogen, V_{H} is the partial molar volume of hydrogen, σ_{H} is the hydrostatic stress (which will be highest in the neighbourhood of a crack), R is the gas constant, and T is the absolute temperature.

Hydrogen in the bulk of the metal usually intensifies the active deformation processes through mechanisms like hydrogen-enhanced localised plasticity (HELP) and hydrogen-enhanced strain-induced vacancy formation (HESIV) [41, 42, 43, 44]. Moreover, the adsorption-induced dislocation emission (AIDE) mechanism even claims that hydrogen adsorption on the surface leads to more plasticity and thus increased crack initiation by nucleating dislocation on the crack surface, [41, 42]. Finally, also notable from the perspective of active HE, in [45], it was demonstrated through DFT calculations that the adsorption of hydrogen on both the bcc and face-centred cubic (fcc) iron surface stabilized the (100) surface facets by reducing the surface energy, which decreased the force needed to form new (100) surfaces, i.e. hydrogen adsorption on the surface directly contributed to HE rather than only operating from the bulk. This falls within the hydrogen-enhanced decohesion (HEDE) mechanism. It is clear that many complex interactions interplay, both at the surface and in the bulk, and that mitigation of HE via alteration of the surface adsorption kinetics is an important strategy to be looked deeper into.

3. Gaseous inhibitors

3.1. Introduction

Certain gaseous compounds inhibit hydrogen adsorption and dissociation processes on the Fe surface, reducing HE of stressed materials [26]. As previously stated, the Fe surface provides favourable sites for atomic hydrogen adsorption. Physical processes, such as adsorption of molecular hydrogen on the metal surface and dissociation, must occur before atomic hydrogen absorption. Any environmental or mechanical condition that disrupts molecular hydrogen adsorption or hydrogen molecule dissociation on the timescale of stress application can inhibit HE [26]. The efficacy of reducing HE through an impurity gas is closely linked to the occupation of these favourable sites by the impurity gas on the Fe surface. The rate at which the impurity reacts with the Fe surface determines the degree of this occupancy [46]. When hydrogen gas carries impurity molecules containing more electronegative elements than hydrogen, they readily interact with the Fe surface, significantly reducing surface catalytic activity due to electron density localization (catalyst poisoning). As a result, the activation barrier for hydrogen dissociation increases, while the dissociation rate constant decreases by a few orders

of magnitude [25]. The ability of gaseous additives to increase or decrease the supply of hydrogen atoms at the metal surface determines whether they promote or inhibit crack growth. Several experimental surface science studies have shed light on gases like oxygen and carbon monoxide that act as HE inhibitors by interfering with a steel's catalytic activity, preventing the formation of chemisorbed hydrogen atoms on the steel surface. These surface science studies also explain why these gas species act as inhibitors: the presence of C, O, and S in their molecules makes them more electronegative than H, and the presence of unsaturated bonds makes them preferential for electron acceptance/donation. Therefore, the ability of these gas species to inhibit is related to the competition with hydrogen for adsorption sites [26, 47, 48].

In literature, several experimental methods have been employed to investigate the adsorption and dissociation of carbon monoxide (CO) and oxygen (O₂) gas on low-index and high-index iron surfaces since different crystallographic planes behave differently in the presence of gaseous inhibitors. These will be discussed in the next sections.

3.2. Iron-CO Interaction: Surface Dynamics and Preferred Sites

3.2.1. CO surface coverage

Variations in CO surface coverage on the Fe surface result in distinct changes in the heat of adsorption. An intricate balance exists between the surface coverage of CO, the thermodynamic properties governing adsorption, and the diverse adsorption species that contribute to the dynamic behaviour of the system [27, 49]. For instance, when CO covers 50% of the Fe(110) plane, it assumes a distorted configuration, characterized by the presence of tilted and off-centre CO molecules at the top site, cf. Figure 2. This distortion is likely induced by steric repulsion among adjacent CO molecules. As a result, CO never occupies more than 50% of the Fe surface even though the distance between next-nearest-neighbour adsorption sites for CO is sufficient for two CO molecules when they would not be distorted [50, 25, 46].

3.2.2. CO preferred sites

Preferred sites by CO depend on the surface coverage of CO on the given Fe surface, i.e. low index Fe(100), Fe(110), and Fe(111) surfaces and high index Fe(210), Fe(211), and Fe(310) surfaces [27]. The adsorption configuration of CO, binding strength, dissociation energies,

and dissociation barriers on these Fe surfaces dictate the strength of adsorption of CO onto the Fe surface, [25, 51]. At high coverage of CO, the dissociation of incoming CO molecules depends on the C-O bond length, activation energies and the transition states of the dissociated CO governed by the prevailing thermodynamic and kinetic state of the Fe-CO system [27]. The dissociative adsorption of CO on the iron surface is dependent on the activation barriers. A correlation exists where the activation barrier decreases with decreasing planar density of iron. Specifically, the sequence follows Fe(111) > Fe(100) > Fe(110) [27, 52]. The preferred adsorption sites for C and O atoms on Fe(110) are the long-bridge (LB) site for C and the quasi-3-fold (TF) and LB sites for O, [50]. The CO molecule exhibits the most robust binding to the Fe(001) surface at the 4-fold hollow site, cf. Figure 2 [27, 53].

3.2.3. CO-H co-adsorption

Carbon monoxide interaction with the Fe surface forms a partial monolayer on the Fe surface [25]. The level of CO surface coverage influences the H₂ dissociation energy and H subsurface migration activation energy [25]:

- H₂ dissociation energy : The electron-donating capacity of an Fe surface plays a crucial role in its catalytic activity for electrophilic reactions. High CO surface coverage diminishes available electron density, reducing the surface's ability to donate electrons to chemisorbed electronegative species. This results in an increased hydrogen dissociation energy and an activation barrier for dissociation, rendering CO a catalytic poison to the Fe surface [25, 46]. Despite the barrier leading to a lower H₂ dissociation rate under normal conditions, prolonged exposure or external stimuli, such as applied pressure, gradually increases the surface concentration of atomistic hydrogen, inducing HE. In contrast to CO interaction, the interaction of hydrogen with the Fe surface exhibits a different dependence. The ability to dissociate new hydrogen molecules at a constant rate persists, unaffected by surface-adsorbed molecular hydrogen, although the initially high rate constants equilibrate over time and remain constant [46].

- H subsurface migration activation energy : Surface layers with low CO surface coverage are electron-rich and have a high interatomic electron density. As a result, the electron density would act as an effective barrier to hydrogen entry into the material. However, when there is a lot of CO adsorbed on the surface, the surface layers are electron-poor and have a low interatomic electron density. The low electron density would significantly lower the barrier to hydrogen migration from the surface to the subsurface in the event that a hydrogen molecule is able to dissociate on the CO covered surface, Figure 3 [25].

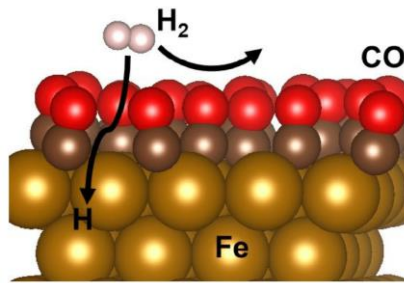


Figure 3: CO-H co-adsorption, reproduced from [25]

3.3. Iron-O₂ Interaction: Surface Dynamics and Preferred Sites

3.3.1. O₂ surface coverage

Like CO, the adsorption of oxygen (O₂) on Fe(110) depends on the surface coverage of O₂. The change in adsorption energy resulting from oxygen adsorption on the Fe(110) surface is influenced by variations in the height of O₂ above the surface and the Fe-O bond length [54]. Experimental and computational model observations indicate that O₂ spontaneously adsorbs on Fe(110) and Fe(100) surfaces without requiring external activation energy (non-activated) up to a coverage of 1 monolayer (a monolayer is a complete layer of O atoms on the Fe surface) [55]. Conversely, in dissociative adsorption, where molecular oxygen breaks into individual atoms during adsorption, this remains a non-activated process only for lower coverages, specifically below 0.5 monolayers [55, 56]. Beyond this coverage threshold, dissociative adsorption becomes activated, suggesting additional energy input is needed when the surface coverage is higher.

3.3.2. *O₂ preferred sites*

First-principles studies of oxygen adsorption on the Fe(110) surface reveal the stability of all high-symmetry sites (3-fold-hollow, long-bridge, short-bridge, top, cf. Figure 2) for both low and high oxygen coverages. The binding of the adsorbate is weaker in short-bridge and top positions. The 3-fold-coordinated hollow sites emerge energetically as the most favoured across all coverage scenarios. At low coverage, oxygen adsorption energy in the 3-fold hollow and long-bridge sites is comparable. In contrast, at high coverages, the binding strength of oxygen in a 3-fold hollow site exceeds that in a long-bridge position [54, 57]. For the Fe(100) surface, the most stable adsorption site is the hollow site, with the bridge and top sites being less stable [58].

3.3.3. *O₂-H co-adsorption*

Oxygen is more electronegative than hydrogen. Due to greater electronegativity, oxygen molecules are attracted to the Fe surface easier than hydrogen molecules. This results in a higher concentration of O₂ near the Fe surface than in the gas bulk, which facilitates the surface-electron transfer and catalyses the dissociation reaction. The dissociation of O₂ occurs without the formation of a stable precursor state or an activation barrier, thus making it faster. Oxygen atoms on the surface withdraw and localize electron density, limiting the ability of Fe atoms on the surface to donate electrons to the hydrogen molecule. As a result, H₂ has less access to electron density, and the dissociation of molecular hydrogen is impeded [26].

Pre-adsorbed oxygen can alter the properties of the surface from attractive to repulsive. The activation barrier for hydrogen dissociation increases due to the presence of oxygen atoms and hinders the surface catalytic activity. O₂ competes effectively with H₂, and after dissociation, the oxygen atoms on the surface repel H₂ molecules to the gas bulk. Since O₂ is more electronegative than CO, the inhibiting effect on H₂ dissociation is stronger than CO [26]. From [29], the oxygen adsorption experiments revealed that the majority of the adsorbed oxygen was desorbed by evacuating the system. The small amount of oxygen (0.7 μg) that remained adsorbed did not affect subsequent hydrogen adsorption. However, it was noticed that when both O₂ and H₂ were present in the gas phase, even for small amount of oxygen (0.33 kPa as compared to the total pressure of 33 kPa), hydrogen adsorption was slowed. In their research, Hancock and

Johnson [59] demonstrated that hydrogen at atmospheric pressure and room temperature has the potential to induce subcritical crack growth (SCG) in H11 tool steel. Their findings revealed that even a small amount of O₂ as an impurity in hydrogen gas could stop a growing sub-critical crack by adsorbing on fresh surfaces. Furthermore, when the O₂-containing atmosphere was replaced with pure hydrogen, SCG was restored, often requiring minor mechanical stimulation. This suggests that the process of hydrogen adsorption involves breaking the adsorbed O₂ surface layer. Therefore, the higher electronegativity of O₂ accelerates its dissociation, impeding the surface catalytic activity and hindering the efficient dissociation of hydrogen molecules on the Fe surface.

4. Mechanical validation of hydrogen embrittlement mitigation by gaseous inhibitors

4.1. Inhibitor efficiency assessment

This section delves into assessing inhibitor efficiency of potential inhibitor gases through fracture toughness and fatigue tests. These examinations explore the impact of H₂ on both the mechanical properties and the characteristics of potential inhibitors within specific materials. Various factors, like gas pressure, temperature, loading rate, and loading type influence the inhibitory efficiency. An overall comparison among different inhibitors is made in [60], for 2.25Cr - 1Mo steel. Fatigue tests were done at stress intensity factor $\Delta K = 24 \text{ MPa } m^{1/2}$, frequency = 5 Hz, load ratio = 0.1 in the presence of 1.1 MPa H₂ gas, figure 4. The figure shows the ratio of the fatigue crack growth rate (FCGR) in hydrogen gas containing additives to the FCGR in pure hydrogen gas. A ratio of 1.0 indicates that the FCGR in the two environments were equal. The data showed that low concentrations of oxygen and carbon monoxide gas can mitigate HE. Other than CO and O₂, there is evidence in literature for inhibitors like N₂O and NH₃ that significantly reduce crack propagation in martensitic steels [47]. In contradiction, gases like methyl mercaptan and hydrogen sulfide can exacerbate HE. In [61], it is discussed that the effect of methyl mercaptan (CH₃SH) as an inhibitor or promoter of HE depends on the material. CO₂, CH₄, and C₂H₂ show minimal impact, where it is claimed that CO₂ and CH₄ compete less favourably with H₂ for adsorption sites and C₂H₂ dissociates into H₂ [47]. Studies from [62] highlight that a mixture of CO, CO₂, and CH₄ inhibitors in H₂ gas have similar fracture

toughness for API 5L X42 and API 5L X70 pipeline steels compared to that in air. Additionally, inhibitors like SO₂ and C₂H₆ moderately slow down crack growth in X42 pipeline steel [62]. Given the undeniable potential of CO, O₂ and NH₃, the next sections are devoted to these inhibitor gases discussing the influence of various parameters on the inhibitor efficiency.

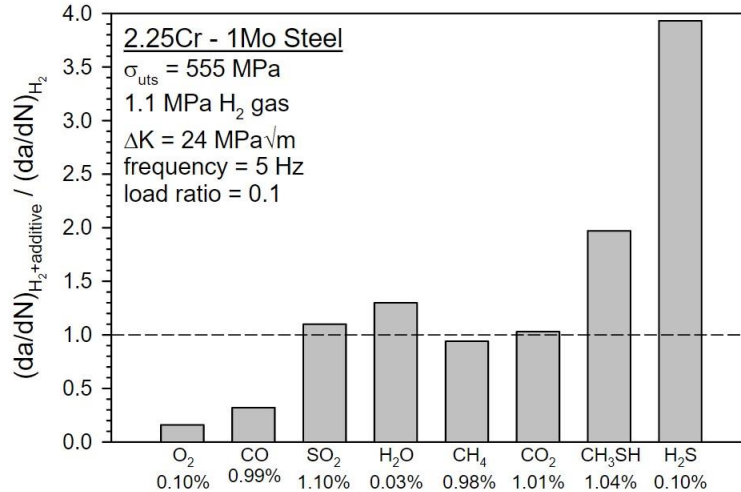


Figure 4: Effect of gas additives on the fatigue crack growth rate (da/dN) at constant stress intensity factor range (ΔK) for a low-alloy steel in hydrogen gas. Reproduced from [60].

4.2. Influencing factors to CO inhibition

4.2.1. CO concentration

Figure 5 shows results of fatigue crack growth tests conducted on ASTM A333 pipeline steels at room temperature under a gas pressure of 0.11 MPa. The tests were performed at loading frequencies of 20Hz and 0.02Hz, with a load ratio (R) of 0.1 [63]. A333 steel has a ferrite-pearlite microstructure, which is ordered in bands in the longitudinal and transverse directions. Focusing on one loading frequency only, Figure 5a shows the FCGR curves in different environments with reference to air and pure H₂ at 20Hz. In the presence of CO, at 1000 vppm CO added to H₂, the FCGR curve follows that of high purity H₂. At 10,000 vppm of CO added to H₂, the FCGR started accelerating at the same ΔK as that of pure H₂, but the amount of acceleration was less (i.e. the crack growth rate was less than that at H₂ + 1000 vppm CO). At 100,000 vppm of CO added to H₂, there was an increase in critical ΔK to around 21 MPa $m^{1/2}$ (corresponding to the onset of hydrogen accelerated fatigue crack growth as reported to be 5 x

10^{-8} m/cycle). Thus, up to a CO content of 10,000 vppm, the ratio of acceleration is first reduced with the same critical ΔK and eventually at 100,000 vppm CO the onset of the acceleration is shifted to higher ΔK . The competition between the rate of CO surface coverage and the rate of fresh surface creation determines the inhibitory effect of CO. With the increase in CO content, the rate of CO surface coverage increased to an equivalent or higher value compared to the rate of fresh surface creation. It is noticeable that the FCGR below critical ΔK for mixtures of CO and H₂ is lower than that in air. This is stated to be related to water vapour in the air providing H atoms [64, 65].

4.2.2. Loading frequency

Building upon the mechanical test discussed in the preceding subsection [63], when comparing figure 5a with figure 5b, showing FCGR curves at a frequency of 0.02Hz for similar gas environments, the effect of the loading frequency can be evaluated. In the high purity H₂ environment at a frequency of 0.02Hz, the accelerated FCGR occurs at a critical $\Delta K = 12 \text{ MPa } m^{1/2}$ and the ratio of acceleration is 18, while the critical $\Delta K > 17 \text{ MPa } m^{1/2}$ at 20Hz with a ratio of 6.5. This suggests that at lower frequencies, the effect of hydrogen became more significant given the earlier onset of acceleration (ΔK where there is a significant increase in the crack growth rate) and a higher rate of acceleration ($(da/dN)_{H_2} / (da/dN)_{air}$). This can be understood as the hydrogen had more time to diffuse to the crack tip vicinity due to more prolonged testing times at lower frequencies [66, 67]. It should be noted that the observed increase in the hydrogen effect at lower frequencies cannot be generalised since Matsunaga et al. [68] indicated that for certain hydrogen partial pressures, FCGR decreased with decreasing frequency, which might be due to the hydrogen concentration gradient on the one hand and the covering of the crack tip by oxygen (might be other inhibitors as well) on the other hand. The presence of CO did not exhibit any inhibitory effect in the lower ΔK range. However, in the higher ΔK range, the inhibitory impact of CO became noticeable. The crack growth rate decreased at high ΔK values due to the inhibitory effect of CO. The effect was more significant with an increase in the CO content, which was also concluded based on the 20 Hz results. However, the inhibitory effect of CO became obvious at lower CO contents for lower test frequencies which can again be explained by the more prolonged testing time at lower frequencies leading to more time for

CO to adsorb on the surface. Eventually, for both 1,000 and 10,000 vppm of CO at a frequency of 0.02 Hz, a constant FCGR was achieved. The interplay between hydrogen supply via diffusion in the material and CO adsorption speed on the surface resulted in this constant crack growth rate for mixtures of CO and H₂.

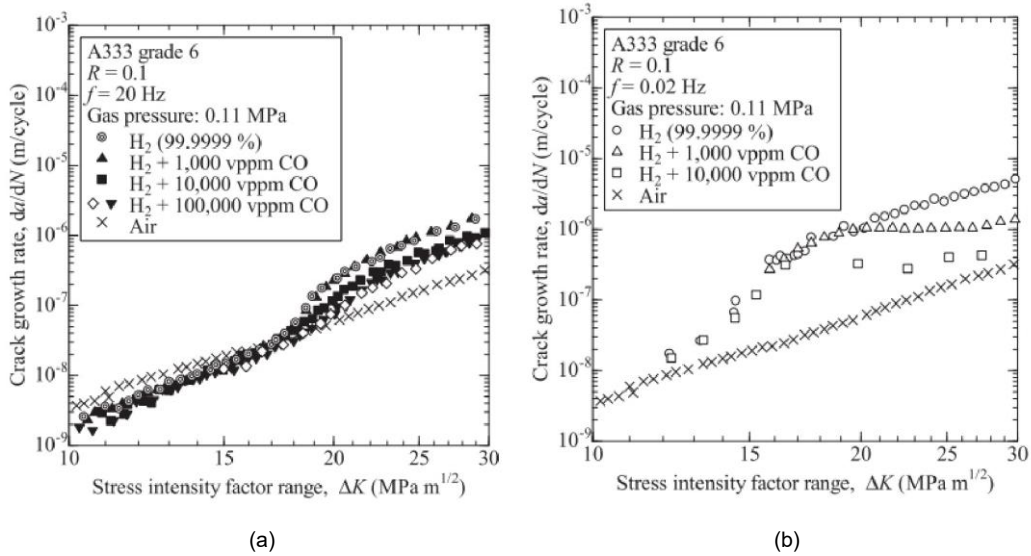


Figure 5: Inhibition effect of CO under varying concentrations at a frequency of: a) 20 Hz, and b) 0.02 Hz. Reproduced from[63].

4.2.3. Crosshead speed

Figure 6 illustrates the dependency of the inhibitory effect of carbon monoxide (CO) on the loading rate in a fracture toughness test conducted on pure iron [25]. The test was carried out under an environmental gas pressure of 0.6 MPa and a temperature of 293 K. As a reference, a test was performed in pure N₂ at a loading rate of 2x10⁻³ mm/s, resulting in a steeper J-integral curve. A significant reduction in the slope of the J-integral was observed for the test conducted in pure H₂ at a loading rate of 2x10⁻³ mm/s, highlighting the embrittlement effect caused by hydrogen. To assess the effectiveness of CO in inhibiting HE, fracture toughness tests were conducted at two different loading rates: 2x10⁻³ mm/s and 2x10⁻⁵ mm/s, with a gas mixture consisting of H₂ + 1000 vppm CO. At the higher loading rate of 2x10⁻³ mm/s, the J-integral curve was comparable to that in pure N₂, indicating successful mitigation of HE. However, at the lower loading

rate of 2×10^{-5} mm/s, the slope of the J-integral curve was less than that of 2×10^{-3} mm/s. This decrease in the slope of J-integral curve at the lower loading rate can be attributed to incomplete CO coverage on the iron surface, facilitating hydrogen entry into the material.

As discussed in Section 3.2.1, achieving 100% CO coverage on the iron surface is thermodynamically challenging. Additionally, at the 2×10^{-5} mm/s loading rate, prolonged exposure times to H_2 provided sufficient time for hydrogen to absorb into the material. Thus, due to the incomplete surface coverage by CO and extended exposure time for H_2 permeation, the efficiency of CO inhibition decreased with decreasing loading rate.

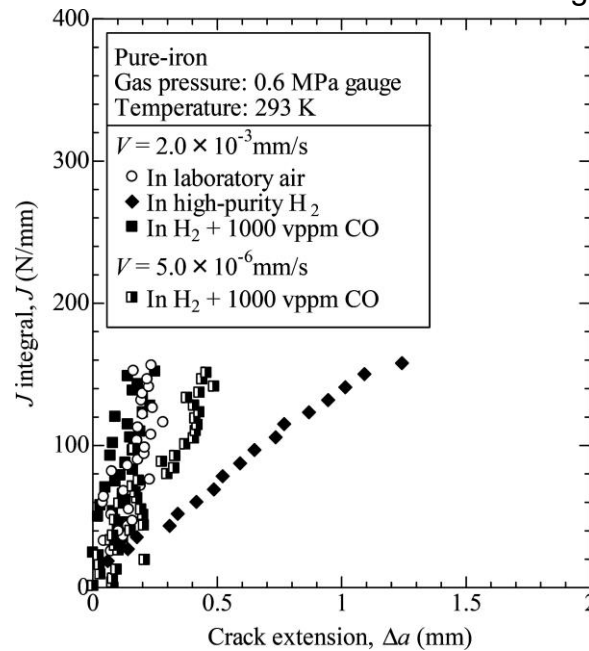


Figure 6: Inhibitory effect of CO on hydrogen embrittlement and its loading rate dependency. Reproduced from [25].

4.2.4. Environmental gas pressure

Figure 7 and figure 8 present results of fracture toughness tests conducted on ASTM A106 grade B pipeline steels at 293K at three different gas pressures of 0.6 MPa, 1 MPa and 4 MPa. The tests were performed at a constant crosshead speed of 2.0×10^{-3} mm/s, [46]. A106 pipe carbon steel has a banded ferrite-pearlite microstructure in the longitudinal and transverse directions as well. Figure 7a depicts the effect of H_2 gas pressure on resistance curves (expressed as J-integral versus stable

crack extension Δa) in high-purity H_2 . Regardless of the applied pressure, all the J - Δa curves in high-purity H_2 are very consistent with each other and located significantly lower than the J - Δa curves in high-purity N_2 . In general, steels become more susceptible to HE as the H_2 gas pressure increases because the hydrogen entry into the material increases. However, above certain H_2 gas pressures, hydrogen saturation is reached. The hydrogen trap sites associated with the fracture are fully occupied by hydrogen, already at 0.6 MPa, which is one of the reasons for the similar fracture toughness values regardless of varying hydrogen pressure. Similar tendencies are also seen in [7, 69, 70], where the FCGR is insensitive to hydrogen gas pressure beyond a certain value depending on the testing conditions and the material microstructure. Figures 7b and 8a depict the J - Δa curves obtained from fracture toughness tests in CO mixed H_2 gases at 0.6 MPa and 4 MPa environmental gas pressure, respectively. The mitigation effect of CO on HE susceptibility increased as the CO content in the H_2 gas environment increased, which is similar to what was discussed in section 4.2.1. However, the mitigation effect of CO decreased as the overall gas pressure increased at a particular CO content and the given crosshead speed. Thus, the CO content required to inhibit H dissociation/adsorption increased. This is clearly summarized in figure 8b, where instead of the total pressure of the gas environment, H_2 gas partial pressure is considered. This confirms the positive dependence of CO content on the H_2 gas partial pressure required to inhibit HE.

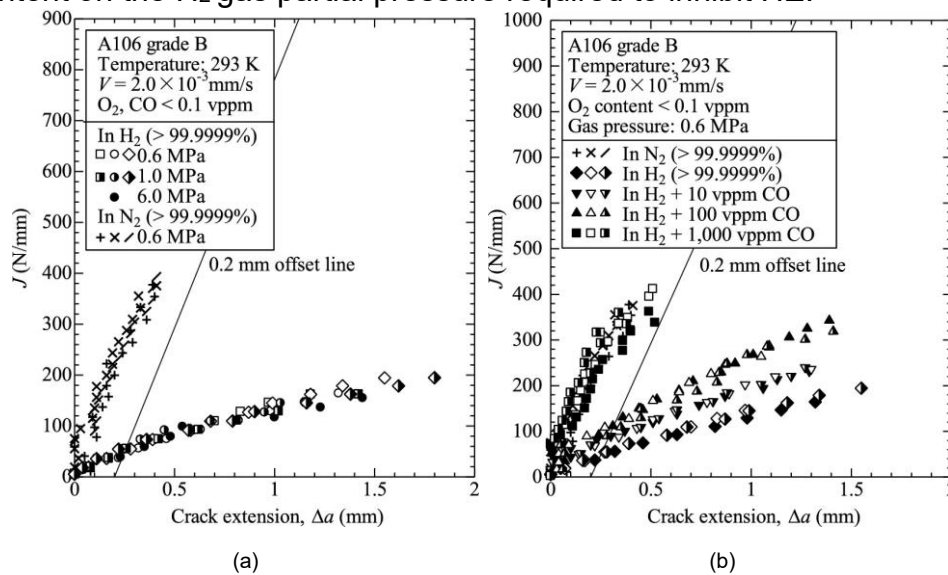


Figure 7: a) Effect of H₂ gas pressure on J-Δa curves of A106 grade B carbon steel in pure H₂ versus purity N₂ gas. b) Effect CO on fracture toughness and crack extension at 0.6 MPa in CO-H mixture. Reproduced from [46].

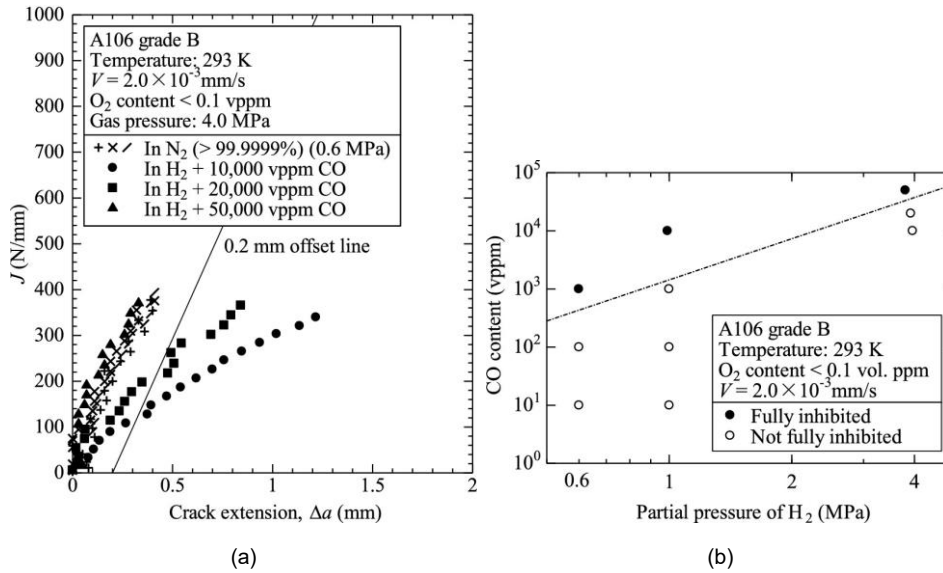


Figure 8: a) Effect of CO on fracture toughness and crack extension at 4 MPa in CO-H mixture. b) Effect of H₂ partial pressure on the threshold CO content preventing HE. Reproduced from [46].

4.3. Influencing factors to O₂ inhibition

4.3.1. O₂ concentration

Figure 9 shows fracture toughness tests that were carried out on A333 pipeline steels at 293K at three different crosshead speeds of 2x10⁻³ mm/s, 2x10⁻⁴ mm/s and 2x10⁻⁵ mm/s and three different O₂ contents of 100, 10 and 0.1 vppm. The tests were conducted under an H₂ gas pressure of 0.6MPa, [71]. Figure 9a shows the tearing resistance curve, i.e. the relationship between J-integral and crack extension Δa. The inhibitory effect of oxygen gas is very prominent in these graphs. For a crosshead speed of 2x10⁻³ mm/s, increasing the O₂ content to 10 vppm partially inhibited the H₂ effect. When the O₂ content was 100 vppm, there was little or no reduction in fracture toughness and the curve was similar to that in air. This is consistent with the studies done in [48], where the increased O₂ content prevented H₂ interaction when the material was subjected to fracture tests. Figure 9b shows early stage J-Δa curves. In this figure,

initially, the curves of air and 10 vppm O₂ coincide. At 30 μm crack length, the slope of J-Δa in H₂ with 10 vppm O₂ decreased and deviated from the one in air. This observation confirms that O₂ can prevent the effect of H₂ up to a certain extent, i.e. showing partial inhibition.

The crack tip shape in Figure 10 illustrates the inhibitory effect of O₂. As depicted in Figures 10a and d, an increase in O₂ content leads to an enhanced blunting of the crack tip, resulting in micrographs similar to those observed in air. In Figure 10b, the crack tip appears sharp in the presence of H₂ + 0.1 vppm O₂. Meanwhile, in Figure 10c, the crack tip undergoes a gradual transition from blunt to sharp. This phenomenon is attributed to the partial inhibition of O₂. In all testing environments, the inhibitory effect of O₂ is associated with the rate at which a newly formed surface is passivated by O₂.

The crack tip strain rate theory, as outlined in [72], provides insights into this behaviour. The time interval between crack extensions (rupture events) is determined by the ratio of surface layer rupture strain to crack tip strain rate. As the strain rate increases (for example due to a higher crosshead speed in the tensile load setup), the time between successive rupture events decreases, leading to a reduced rate of oxygen repassivation. Consequently, the newly formed surface ahead of the crack tip becomes susceptible to hydrogen, accelerating crack growth [72]. This is particularly evident in the testing environment with 10 vppm of O₂, where initially, passivation of the new surface formed ahead of the crack tip was effectively done by O₂. The competition between the rate at which a new surface is created and the rate at which it is covered by O₂ is crucial. When the rate at which O₂ covers the surface is higher than the rate at which a new surface is created, O₂ inhibits hydrogen degradation. However, when the rate at which O₂ covers the surface is slower than the rate at which a new surface is created, the hydrogen effect is observed in the form of a sharper crack tip. Thus, O₂ is unable to inhibit hydrogen degradation effectively in such cases.

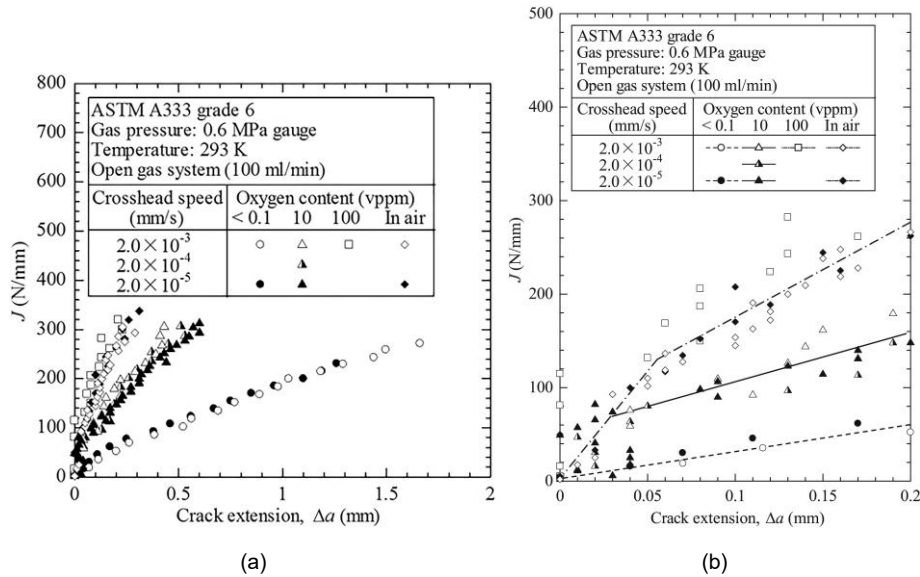


Figure 9: J- Δa curves in H₂ with different O₂ contents and crosshead speeds, a) overview, b) at an early stage of the fracture toughness test. Reproduced from [71].

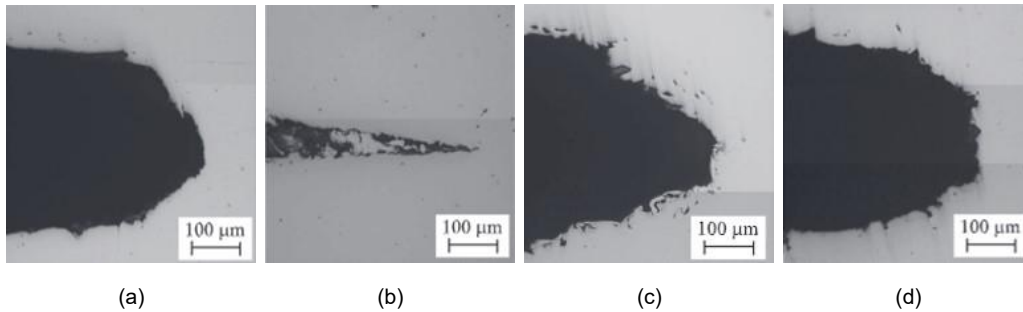


Figure 10: a) Crack tip shape in air at a crosshead speed of 2×10^{-3} mm/s; Change in the crack tip shape because of the effects of hydrogen and the addition of b) 0.1 vppm c) 10 vppm d) 100 vppm of O₂ to the H₂ gas at a crosshead speed of 2×10^{-3} mm/s. Reproduced from [71].

4.3.2. Loading frequency

Fatigue crack growth rate (FCGR, da/dN) tests were done on a low strength line pipe steel (X52) in high-pressure H₂ gas. The FCGR was measured as a function of the ΔK range, load cycle frequency, load ratio (e.g. mean stress) and O₂ concentration [72]. The microstructure consists of ferrite and pearlite with bands of inclusions concentrated at the mid-

thickness of the pipe wall. Two fatigue crack growth test methods were applied: constant load frequency and constant ΔK . Under constant load frequency, the aim was to measure the crack growth rate as a function of ΔK , whereas, under constant ΔK , the aim was to measure the crack growth rate as a function of frequency. Figure 11 shows da/dN vs load cycle frequency relationship at $R = 0.1$ for H_2 and O_2 environments. At lower frequencies, the data points coincide with air whereas, at higher frequencies, there is a marked rise in da/dN . Further, da/dN increases sooner for 10 vppm of O_2 than for 100 and 1000 vppm of O_2 . Thus, at higher frequencies, the passivation rate by O_2 decreased and da/dN increased. This was also claimed in [73], where fatigue tests on X100 pipeline steel in a mixed environment of $H_2 + 100$ vppm O_2 at 2.1 MPa gas pressure for a load ratio of 0.1 were done at frequencies of 1 Hz and 10 Hz. No crack growth was seen for 1 Hz whereas 10 Hz showed a critical da/dN that activated the fatigue crack growth. The rate of new crack tip surface creation, influenced by load cycle frequency, became crucial, affecting the time required for observed effects. Under constant ΔK testing, frequency dependence emerges, with higher frequencies promoting increased surface creation.

The crack tip blunting and resharpener theory [72], focuses on the impact of loading and unloading cycles on crack growth behaviour in fatigue testing. During the loading phase, the crack tip blunts, creating a new surface that is subsequently passivated by oxygen. This passive layer is assumed to form continuously throughout the loading-unloading cycle. In the unloading phase, the crack tip undergoes resharpener, causing the rupture of the passive layer as the crack advances. The load cycle period represents the time between rupture events when oxygen is involved in passivating the newly formed surface, [72]. The competition between oxygen-induced passivation and hydrogen-accelerated fatigue crack growth is time-dependent, with higher frequencies (less time between loading and unloading) making passivation by oxygen challenging. This emphasizes the role of frequency in influencing these dynamics.

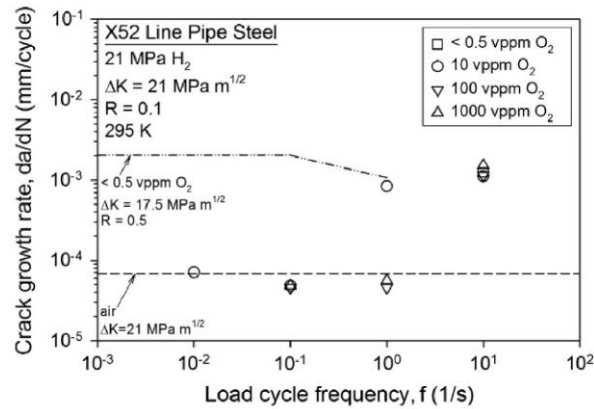


Figure 11: da/dN vs. load cycle frequency (f) for X52 line pipe steel in mixed $H_2 + O_2$ gases at $R = 0.1$ and $\Delta K = 21 \text{ MPa } m^{1/2}$. The crack growth rate in high-purity H_2 ($< 0.5 \text{ vppm } O_2$) at 10 Hz and in air are shown for comparison at $\Delta K = 21 \text{ MPa } m^{1/2}$. The trend line for air was included to contrast the da/dN vs. f behaviours in high-purity H_2 and mixed $H_2 + O_2$ gases in the lower range of f . Reproduced from [72].

4.3.3. Crosshead speed

Expanding on the mechanical test result of the previous subsection 4.3.1 [71], in general, the effect of H_2 becomes more pronounced as the crosshead speed decreases because the amount of H_2 that permeates the material up to a certain crack extension increases. In figure 9a, however, there is no significant difference between the resistance curves at a crosshead speed of $2 \times 10^{-3} \text{ mm/s}$ and $2 \times 10^{-5} \text{ mm/s}$. Thus, in the relatively low loading rate region (low crosshead speeds), the effect of H_2 is independent of the loading rate due to sufficient H_2 entering and saturating the material [71]. In [71], the effect of crosshead speed on the O_2 inhibitory effect is also negligible since, independent of the applied crosshead speed, the 10 vppm curves more or less coincided. It should be noted, however, that more data at other O_2 contents is lacking to make conclusions on this parameter influence.

4.3.4. Stress intensity factor range ΔK

Extending on the parameters of the mechanical tests from the preceding subsection 4.3.2 [72], Figure 12 shows the da/dN vs ΔK relationships for various H_2 and O_2 environments at 10 Hz frequency and $R = 0.1$. In comparison to the da/dN vs ΔK curves in air and high-purity H_2 ,

the transition point to accelerated crack growth for H₂ and O₂ environments has shifted to higher ΔK values depending on the O₂ content.

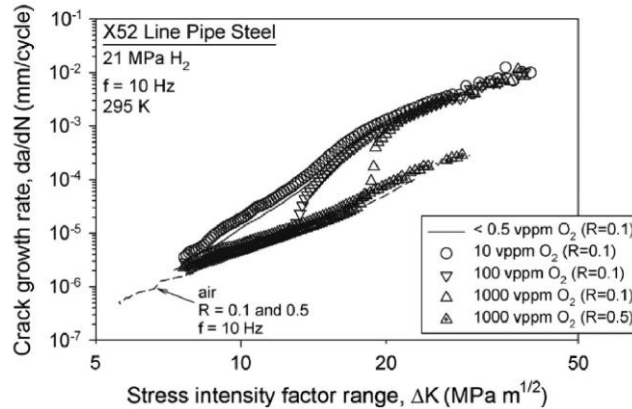


Figure 12: da/dN vs ΔK relationships for X52 line pipe steel in mixed H₂ + O₂ (R = 0.1 or 0.5), high-purity hydrogen gas (R = 0.1), and ambient air (R = 0.1 and 0.5). Reproduced from [72].

4.4. Influencing factors to NH₃ inhibition

Another probable candidate as a gaseous inhibitor is NH₃. Added to gaseous hydrogen in trace amounts, NH₃ reduces the embrittling effect of atomic hydrogen, as discussed further. An additional advantage is that it is carbon-free. Hence, the following sections delve into assessing NH₃ as a gaseous inhibitor for gaseous hydrogen transport.

4.4.1. Crosshead speed

Fracture toughness tests were done on Cr-Mo low alloy steel with a tempered martensite microstructure at 293K [74]. The used crosshead speeds were 2x10⁻³ mm/s, and 2x10⁻⁵ mm/s and the total pressure of the environmental gases were 0.1MPa and 1MPa. Figure 13 shows the results of these tests presented as J- Δa curves for the pressure of 0.1MPa. Like O₂ and CO, there is preferential adsorption of NH₃ on the steel surface. This leads to a clear deviation for the pure H₂ curve, i.e. NH₃ is able to act as an inhibitor. However, when NH₃ is added to pure N₂ gas, a similar behaviour is observed as the H₂ + NH₃ mixture. The explanation can be found in the decomposition of NH₃ which also serves as a source of hydrogen. The rate of hydrogen production is, however, lower than for pure H₂ [29, 75]. As the loading rate was reduced, the fracture toughness was

reduced drastically in the presence of hydrogen. When NH_3 was present, both in a nitrogen and hydrogen environment, significant reduction in fracture toughness was observed, figure 13b, albeit to a lesser extent compared to that in pure hydrogen. The decrease in the loading rate to 2.0×10^{-5} mm/s led to sufficient time for NH_3 decomposition (that produces some hydrogen) and hydrogen diffusion to the crack tip to cause HE. When the loading rate was 2.0×10^{-3} mm/s, the level of HE was much more limited due to the low rate of NH_3 decomposition.

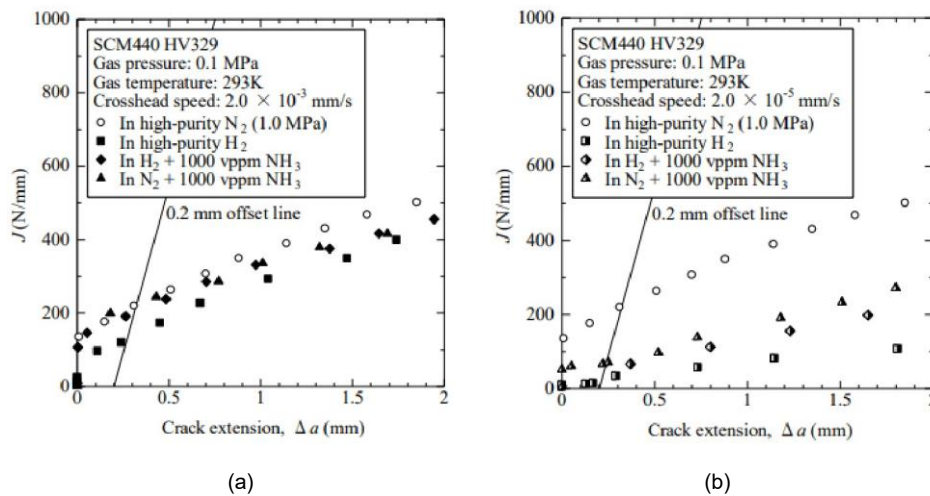


Figure 13: Effect of NH_3 addition to the testing environment on J- Δa curve at $p_T = 0.1$ MPa and crosshead speed : a) 2.0×10^{-3} mm/s and b) 2.0×10^{-5} mm/s. Reproduced from [74].

4.4.2. Environmental gas pressure

Building upon the mechanical test parameters elucidated in the preceding subsection [74], figure 14 shows the fracture toughness test results for a pressure of 1 MPa and a crosshead speed of 2.0×10^{-3} mm/s. Compared to Figure 13a, it can be concluded that the critical value of J-integral, J_{IC} in $\text{H}_2 + \text{NH}_3$ was similar to that in H_2 . J_{IC} is determined where the offset line crosses the resistance curve. Thus, with an increase in total gas pressure, the inhibitory effect of NH_3 disappeared which was related to the increase of the reaction rate of H_2 (Sievert's law) dominating the hydrogen adsorption. In $\text{NH}_3 + \text{N}_2$ mixture, on the contrary, no reduction in J_{IC} was observed for a higher total gas pressure, which implies that the reaction rate of NH_3 decomposition was insufficient to cause a critical amount of hydrogen to absorb in the lattice at a fixed loading rate.

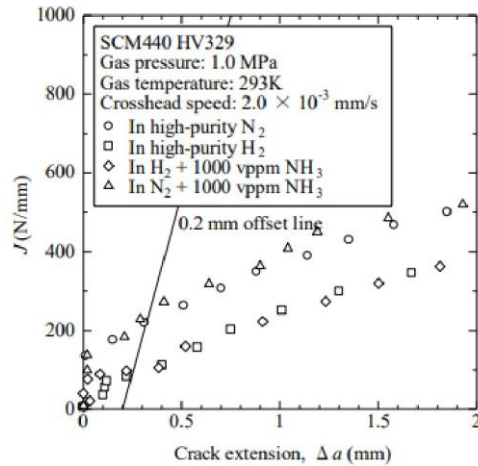


Figure 14: Effect of NH_3 addition to the testing environment on J- Δa curve at $p_T = 1$ MPa and crosshead speed, 2.0×10^{-3} mm/s. Reproduced from [74].

5. Conclusion and suggestions

This work highlighted a comprehensive understanding of gaseous inhibitors in limiting HE in pipeline steels. The following conclusions can be drawn from the present work:

- More electronegative gaseous species compared to the hydrogen molecule are capable of reducing hydrogen adsorption kinetics without affecting hydrogen equilibrium. A continuous inhibitor supply is essential for sustained mitigation.
- Increasing the inhibitor concentration improved the level of HE mitigation.
- Decreasing the loading frequency in fatigue crack growth tests promoted the inhibiting effect, determined by the rate at which inhibitor species can re-adsorb the surface.
- There is a positive dependency of the required inhibitor concentration on the environmental gas pressure.
- Lower crosshead speeds in quasi-static fracture toughness tests reduced the inhibitory effect: for CO due to incomplete surface

coverage allowing hydrogen permeation and for NH₃ due to the production of hydrogen.

The present work yields the following suggestions:

- It is important to consider the techno-economic aspects of mixing inhibitor gases with H₂. While the consistent supply of high-pressure H₂ with inhibitors might be feasible from a technical standpoint, the economic viability of transporting high-pressure gas poses a challenge due to compressibility considerations and associated operational costs on a full scale.
- The current literature has limited experimental results, which necessitates further research and exploration in this field. Exploring various conditions such as temperature fluctuations, hydrogen pressure changes, and varying inhibitor gas contents will lead to the uncovering of key parameters influencing inhibitor efficiency. These experimental data will complement and validate the existing models, opening pathways for enhanced comprehension of their performance in practical applications.

6. Acknowledgements

The authors would like to acknowledge the financial support of the Energy Transition Fund via the HyFit and HySource projects in collaboration with Fluxys. The research was also supported by FWO (post-doctoral fellow project number - 1248122N).

References

- [1] G. Erbach, European green deal - European parliament, 2019. URL: [https://www.europarl.europa.eu/RegData/etudes/ATAG/2019/644205/EPRS_ATA\(2019\)644205_EN.pdf](https://www.europarl.europa.eu/RegData/etudes/ATAG/2019/644205/EPRS_ATA(2019)644205_EN.pdf).
- [2] UNFCCC, The Paris agreement - unfccc, 2018. URL: https://unfccc.int/sites/default/files/resource/parisagreement_publication.pdf.
- [3] EHB European Hydrogen Backbone, 2021. URL: <https://ehb.eu/page/publications>.

- [4] M. W. Melaina, O. Antonia, M. Penev, Blending hydrogen into natural gas pipeline networks: A review of key issues (2013). URL: <https://www.osti.gov/biblio/1068610>. doi:10.2172/1068610.
- [5] B. P. Somerday, C. W. San Marchi, Effects of hydrogen gas on steel vessels and pipelines., Technical Report, Sandia National Lab.(SNLCA), Livermore, CA (United States), 2006.
- [6] N. Nanninga, A. Slifka, Y. Levy, C. White, A review of fatigue crack growth for pipeline steels exposed to hydrogen, *Journal of Research of the National Institute of Standards and Technology* 115 (2010) 437–452. doi:10.6028/jres.115.030.
- [7] C. San Marchi, B. Somerday, Technical reference for hydrogen compatibility of materials, Sandia National Laboratories (2012).
- [8] O. Todoshchenko, Y. Yagodzinskyy, H. Hänninen, Hydrogen uptake and embrittlement susceptibility of ferrite pearlite pipeline steels, in: *International Hydrogen Conference (IHC 2016)*, American Society of Mechanical Engineers, 2017. doi:10.1115/1.861387_ch55.
- [9] K. G. Solheim, J. K. Solberg, J. Walmsley, F. Rosenqvist, T. H. Bjørnå, The role of retained austenite in hydrogen embrittlement of super martensitic stainless steel, *Engineering Failure Analysis* 34 (2013) 140–149. URL: <https://www.sciencedirect.com/science/article/pii/S1350630713002537>. doi:<https://doi.org/10.1016/j.engfailanal.2013.07.025>.
- [10] E. Cabanillas, L. Terminiello, N. Cantalejos, R. Versaci, R. Mercader, Mössbauer studies of strain-induced transformation of retained austenite in dual-phase steels, *Materials Science and Engineering: A* 150 (1992) 113–116.
- [11] M. Karlsen, Ø. Grong, M. Søfferud, J. Hjelen, G. Rørvik, R. Chiron, Scanning electron microscopy/electron backscatter diffraction–based observations of martensite variant selection and slip plane activity in super martensitic stainless steels during plastic deformation at elevated, ambient, and subzero temperatures, *Metallurgical and materials transactions A* 40 (2009) 310–320.
- [12] P. Lam, R. Sindelar, T. Adams, Gaseous hydrogen effects on the mechanical properties of carbon and low alloy steels (u),

Proceedings of PVP2007 2007 ASME Pressure Vessels and Piping Division Conference (2007). doi:10.2172/891665.

- [13] M. Kappes, T. Perez, Blending hydrogen in existing natural gas pipelines: integrity consequences from a fitness for service perspective, *Journal of Pipeline Science and Engineering* (2023) 100141. doi:10.1016/j.jpse.2023.100141.
- [14] S. Shipilov, I. Le May, Structural integrity of aging buried pipelines having cathodic protection, *Engineering Failure Analysis* 13 (2006) 1159– 1176. doi:<https://doi.org/10.1016/j.engfailanal.2005.07.008>.
- [15] M. Kappes, T. Perez, Hydrogen blending in existing natural gas transmission pipelines: A review of hydrogen embrittlement, governing codes, and life prediction methods, *Corrosion Reviews* 41 (2023) 319–347. doi:10.1515/corrrev-2022-0083.
- [16] U. S. Meda, N. Bhat, A. Pandey, K. Subramanya, M. Lourdu Antony Raj, Challenges associated with hydrogen storage systems due to the hydrogen embrittlement of high strength steels, *International Journal of Hydrogen Energy* 48 (2023) 17894–17913. doi:10.1016/j.ijhydene. 2023.01.292.
- [17] M. Wetegrove, M. J. Duarte, K. Taube, M. Rohloff, H. Gopalan, C. Scheu, G. Dehm, A. Kruth, Preventing hydrogen embrittlement: The role of barrier coatings for the hydrogen economy, *Hydrogen* 4 (2023) 307–322. doi:10.3390/hydrogen4020022.
- [18] S. Dwivedi, M. Vishwakarma, Hydrogen embrittlement in different materials: A review, *International Journal of Hydrogen Energy* 43 (2018) 21603–21616. doi:10.1016/j.ijhydene.2018.09.201.
- [19] H. Li, R. Niu, W. Li, H. Lu, J. Cairney, Y.-S. Chen, Hydrogen in pipeline steels: Recent advances in characterization and embrittlement mitigation, *Journal of Natural Gas Science and Engineering* 105 (2022) 104709. doi:10.1016/j.jngse.2022.104709.
- [20] X. Li, X. Ma, J. Zhang, E. Akiyama, Y. Wang, X. Song, Review of hydrogen embrittlement in metals: Hydrogen diffusion, hydrogen characterization, hydrogen embrittlement mechanism and prevention, *Acta Metallurgica Sinica* 33 (2020) 759–773. doi:10.1007/s40195-020-01039-7.

- [21] Y.-Q. Zhu, W. Song, H.-B. Wang, J.-T. Qi, R.-C. Zeng, H. Ren, W.C. Jiang, H.-B. Meng, Y.-X. Li, Advances in reducing hydrogen effect of pipeline steels on hydrogen-blended natural gas transportation: A systematic review of mitigation strategies, *Renewable and Sustainable Energy Reviews* 189 (2024) 113950. doi:10.1016/j.rser.2023.113950.
- [22] H. K. D. H. Bhadeshia, Prevention of hydrogen embrittlement in steels, *ISIJ international* 56 (2016) 24–36.
- [23] A. Barnoush, Hydrogen embrittlement, revisited by in situ electrochemical nanoindentation, Ph.D. thesis, Universität des Saarlandes, 2007.
- [24] J. Hoschke, M. F. W. Chowdhury, J. Venezuela, A. Atrens, A review of hydrogen embrittlement in gas transmission pipeline steels, *Corrosion Reviews* 41 (2023) 277–317. doi:10.1515/correv-2022-0052.
- [25] A. Staykov, R. Komoda, M. Kubota, P. Ginet, F. Barbier, J. Furtado, Coadsorption of CO and H₂ on an Iron Surface and Its Implication on the Hydrogen Embrittlement of Iron, *Journal of Physical Chemistry C* 123 (2019) 30265–30273. doi:10.1021/acs.jpcc.9b06927.
- [26] A. Staykov, J. Yamabe, B. Somerday, Effect of hydrogen gas impurities on the hydrogen dissociation on iron surface, *International Journal of Quantum Chemistry* 114 (2014) 626–635. doi:10.1002/qua.24633.
- [27] T. Wang, X.X. Tian, Y.W. Li, J. Wang, M. Beller, H. Jiao, Coverage dependent co adsorption and dissociation mechanisms on iron surfaces from DFT computations, *ACS Catalysis* 4 (2014) 1991–2005. doi:10.1021/cs500287r.
- [28] D. E. Jiang, E. A. Carter, Diffusion of interstitial hydrogen into and through bcc Fe from first principles, *Physical Review B* 70 (2004) 064102. doi:10.1103/PhysRevB.70.064102.
- [29] V. Srikrishnan, P. Ficalora, Selective Adsorption and Hydrogen Embrittlement, *Metallurgical Transactions A* 7 (1976) 1669–1675. doi:10.1007/bf02817884.

- [30] A. Drexler, F. Konert, O. Sobol, M. Rhode, J. Domitner, C. Sommitsch, T. Böllinghaus, Enhanced gaseous hydrogen solubility in ferritic and martensitic steels at low temperatures, *International Journal of Hydrogen Energy* 47 (2022) 39639–39653. doi:<https://doi.org/10.1016/j.ijhydene.2022.09.109>.
- [31] M. Nagumo, Function of hydrogen in embrittlement of high strength steels, *ISIJ International* 41 (2001) 590–598. doi:10.2355/isijinternational.41.590.
- [32] C. S. Marchi, B. Somerday, S. Robinson, Permeability, solubility and diffusivity of hydrogen isotopes in stainless steels at high gas pressures, *International Journal of Hydrogen Energy* 32 (2007) 100–116. doi:<https://doi.org/10.1016/j.ijhydene.2006.05.008>.
- [33] E. Koren, C. M. H. Hagen, D. Wang, X. Lu, R. Johnsen, J. Yamabe, Experimental comparison of gaseous and electrochemical hydrogen charging in X65 pipeline steel using the permeation technique, *Corrosion Science* 215 (2023) 111025. doi:<https://doi.org/10.1016/j.corsci.2023.111025>.
- [34] E. Koren, C. M. H. Hagen, D. Wang, X. Lu, R. Johnsen, Investigating electrochemical charging conditions equivalent to hydrogen gas exposure of x65 pipeline steel, *Materials and Corrosion* 75 (2023) 315–321. doi:<https://doi.org/10.1002/maco.202313931>.
- [35] H. Liu, H. Ya-Lung, P. Ficalora, The control of catalytic poisoning and stress corrosion cracking, *Engineering Fracture Mechanics* 5 (1973) 281–292. URL: <https://www.sciencedirect.com/science/article/pii/0013794473900234>. doi:[https://doi.org/10.1016/0013-7944\(73\)90023-4](https://doi.org/10.1016/0013-7944(73)90023-4).
- [36] Y. Sun, Y. Ren, Y. F. Cheng, Dissociative adsorption of hydrogen at edge dislocation emergence on α -Fe studied by density functional theory, *International Journal of Hydrogen Energy* 48 (2023) 38821–38841. doi:10.1016/j.ijhydene.2023.06.198.
- [37] H. Liu, P. Ficalora, The control of catalytic poisoning and stress corrosion cracking, *Metallurgical Transactions A* 5 (1973) 281–292. doi:10.1016/0013-7944(73)90023-4.

- [38] Z. Xu, P. Zhang, B. Zhang, B. Lei, Z. Feng, Y. Shao, Y. Wang, G. Meng, Effect of tensile stress on the hydrogen adsorption of x70 pipeline steel, *International Journal of Hydrogen Energy* 47 (2022) 21582–21595.
URL:<https://www.sciencedirect.com/science/article/pii/S0360319922018870>. doi:<https://doi.org/10.1016/j.ijhydene.2022.04.266>.
- [39] Z. Xu, P. Zhang, G. Meng, Y. Wang, J. Wang, Y. Shao, F. Wang, Influence of low tensile stress on the kinetics of hydrogen permeation and evolution behavior in alkaline environment, *International Journal of Hydrogen Energy* 47 (2022) 33803–33812.
URL:
<https://www.sciencedirect.com/science/article/pii/S0360319922033948>. doi:<https://doi.org/10.1016/j.ijhydene.2022.07.260>.
- [40] E. Martínez-Pañeda, A. Díaz, L. Wright, A. Turnbull, Generalised boundary conditions for hydrogen transport at crack tips, *Corrosion Science* 173 (2020) 108698. URL: <https://www.sciencedirect.com/science/article/pii/S0010938X20305345>.
doi:<https://doi.org/10.1016/j.corsci.2020.108698>.
- [41] I. M. Robertson, P. Sofronis, A. Nagao, M.L. Martin, S. Wang, D.W. Gross, K.E. Nygren, Hydrogen embrittlement understood - *Metallurgical and Materials Transactions B* 46 (2015) 1085–1103.
URL: <https://link.springer.com/article/10.1007/s11663-015-0325-y#Abs1>. doi:10.1007/s11663-015-0325-y.
- [42] S. Lynch, 2 - hydrogen embrittlement (HE) phenomena and mechanisms, in: V. Raja, T. Shoji (Eds.), *Stress Corrosion Cracking*, Woodhead Publishing Series in Metals and Surface Engineering, Woodhead Publishing, 2011, pp. 90–130. URL: <https://www.sciencedirect.com/science/article/pii/B978184569673350002X>.
doi:<https://doi.org/10.1533/9780857093769.1.90>.
- [43] M. B. Djukic, G. M. Bakic, V. S. Zeravcic, A. Sedmak, B. Rajcic, The synergistic action and interplay of hydrogen embrittlement mechanisms in steels and iron: Localized plasticity and decohesion, *Engineering Fracture Mechanics* 216 (2019) 106528. URL: <https://www.sciencedirect.com/science/article/pii/S0013794418314152>. doi:<https://doi.org/10.1016/j.engfracmech.2019.106528>.

- [44] M. Nagumo, K. Takai, The predominant role of strain-induced vacancies in hydrogen embrittlement of steels: Overview, *Acta Materialia* 165 (2019) 722–733. URL: <https://www.sciencedirect.com/science/article/pii/S1359645418309558>. doi:<https://doi.org/10.1016/j.actamat.2018.12.013>.
- [45] E. J. Song, H. Bhadeshia, D.W. Suh, Effect of hydrogen on the surface energy of ferrite and austenite, *Corrosion Science* 77 (2013) 379–384. doi:<https://doi.org/10.1016/j.corsci.2013.07.043>.
- [46] R. Komoda, M. Kubota, A. Staykov, P. Ginet, F. Barbier, J. Furtado, L. Prost, A. Nagao, Effect of Gas Pressure on Hydrogen Environment Embrittlement of Carbon Steel A106 in Carbon Monoxide Mixed Hydrogen Gas, *Metallurgical and Materials Transactions A*: 53 (2022) 74–85. doi:10.1007/s11661-021-06491-3.
- [47] J. Frandsen, H. Marcus, Environmentally assisted fatigue crack propagation in steel, *Metallurgical Transactions A* 8 (1977) 265–272. doi:10.1007/bf02661639.
- [48] K. Kussmaul, Fracture mechanical behaviour of the steel 15 MnNi 63 in argon and in high pressure hydrogen gas with admixtures of oxygen, *International Journal of Hydrogen Energy* 23 (1998) 577–582.
- [49] G. Wedler, K. Colb, G. McElhiney, W. Heinrich, An investigation of the interaction of co with polycrystalline iron films, *Applications of Surface Science* 2 (1978) 30–42. doi:[https://doi.org/10.1016/0378-5963\(78\)90004-1](https://doi.org/10.1016/0378-5963(78)90004-1).
- [50] D. Jiang, E. A. Carter, Adsorption and dissociation of co on fe(110) from first principles, *Surface Science* 570 (2004) 167–177. doi:<https://doi.org/10.1016/j.susc.2004.07.035>.
- [51] L. Xu, D. Kirvassilis, Y. Bai, M. Mavrikakis, Atomic and molecular adsorption on fe(110), *Journal of Physical Chemistry C* 667 (2018) 54– 65. doi:10.1016/j.susc.2017.09.002.
- [52] L. Gonzalez, R. Miranda, S. Ferrer, A thermal desorption study of the adsorption of co on Fe(110); enhancement of dissociation by surface defects, *Surface Science* 119 (1982) 61–70. doi:[https://doi.org/10.1016/0039-6028\(82\)90187-X](https://doi.org/10.1016/0039-6028(82)90187-X).

- [53] S. K. Nayak, M. Nooijen, S. L. Bernasek, P. Blaha, Electronic structure study of co adsorption on the fe(001) surface, *The Journal of Physical Chemistry B* 105 (2001) 164–172. doi:10.1021/jp002314e.
- [54] T. Ossowski, A. Kiejna, Oxygen adsorption on Fe(110) surface revisited, *Surface Science* 637-638 (2015) 35–41. doi:https://doi.org/10.1016/j.susc.2015.03.001.
- [55] P. Bloński, A. Kiejna, J. Hafner, Oxygen adsorption on the clean and Oprecovered Fe(110) and (100) surfaces, *Journal of Physics: Condensed Matter* 19 (2007) 096011. doi:10.1088/0953-8984/19/9/096011.
- [56] P. Bloński, A. Kiejna, J. Hafner, Dissociative adsorption of O₂ molecules on O-precovered Fe(110) and Fe(100): Density-functional calculations, *Phys. Rev. B* 77 (2008) 155424. doi:10.1103/PhysRevB.77.155424.
- [57] K. Freindl, T. Ossowski, M. Zajac, N. Spiridis, D. Wilgocka-Ślezak, E. Madej, T. Giela, A. Kiejna, J. Korecki, Oxygen adsorption on the Fe(110) surface: The old system – new structures, *The Journal of Physical Chemistry C* 120 (2016) 3807–3813. doi:10.1021/acs.jpcc.5b11177.
- [58] W. Cao, Adsorption of surface active elements on the iron (100) surface a study based on ab initio calculations, Licentiate Thesis, Skolan for industriell teknik och management, Kungliga Tekniska hogskolan (2019).
- [59] G. Hancock, H. Johnson, Hydrogen, oxygen, and subcritical crack growth in a high-strength steel, *AIME MET SOC TRANS* 236 (1966) 513–516.
- [60] B. Somerday, C. San Marchi, Effects of hydrogen gas on steel vessels and pipelines, *Materials for the Hydrogen Economy* (2007) 157–179. doi:10.1201/9781420006070.ch7.
- [61] K. Yokogawa, S. Fukuyama, G. Han, J. He, Hydrogen environment embrittlement of materials for hydrogen energy service, *HYDROGEN ENERGY PROGRESS* 3 (1996) 2291–2296.

- [62] J. Holbrook, 5 - control of hydrogen embrittlement of metals by chemical inhibitors and coatings, in: Gaseous Hydrogen Embrittlement of Materials in Energy Technologies: Mechanisms, Modelling and Future Developments, Woodhead Publishing, 2012, pp. 129–153. doi:10.1533/9780857095374.1.129.
- [63] R. Komoda, K. Yamada, M. Kubota, P. Ginet, F. Barbier, J. Furtado, L. Prost, The inhibitory effect of carbon monoxide contained in hydrogen gas environment on hydrogen-accelerated fatigue crack growth and its loading frequency dependency, *International Journal of Hydrogen Energy* 44 (2019). doi:10.1016/j.ijhydene.2019.09.146.
- [64] P. Liaw, S. Hudak, J. Donald, Influence of gaseous environments on rates of near-threshold fatigue crack propagation in nickel-molybdenum steel, *Metallurgical Transactions A* 13 (1982) 1633–1645. doi:10.1007/bf02644804.
- [65] R. Cooke, P. Irving, G. Booth, C. Beevers, The slow fatigue crack growth and threshold behaviour of a medium carbon alloy steel in air and vacuum, *Engineering Fracture Mechanics* 7 (1975) 69–77. doi:10.1007/bf02644804.
- [66] T. Shinko, G. Hénaff, D. Halm, G. Benoit, G. Bilotta, M. Arzaghi, Hydrogen-affected fatigue crack propagation at various loading frequencies and gaseous hydrogen pressures in commercially pure iron, *International Journal of Fatigue* 121 (2019) 197–207. doi:https://doi.org/10.1016/j.ijfatigue.2018.12.009.
- [67] S. Matsuoka, H. Tanaka, N. Homma, Y. Murakami, Influence of hydrogen and frequency on fatigue crack growth behavior of Cr-Mo steel, *International Journal of Fracture* 168 (2010) 101–112. doi:https://doi.org/10.1007/s10704-010-9560-z.
- [68] M. Hisao, T. Osamu, Y. Junichiro, M. Saburo, Hydrogen-enhanced fatigue crack growth in steels and its frequency dependence, *Philosophical transactions of the Royal Society A* 375 (2017). doi:https://doi.org/10.1098/rsta.2016.0412.
- [69] M. Yoshikawa, T. Matsuo, N. Tsusumi, H. Matsunaga, S. Matsuoka, Effects of hydrogen gas pressure and test frequency on fatigue crack growth properties of low carbon steel in 0.1-90 MPa hydrogen

- gas, Transactions of the JSME (in Japanese) 80 (2014) SMM0254–SMM0254. doi:10.1299/transjsme.2014smm0254.
- [70] K. Xu, Hydrogen embrittlement of carbon steels and their welds, 2012. URL: <https://api.semanticscholar.org/CorpusID:135073998>.
- [71] R. Komoda, M. Kubota, A. Staykov, P. Ginet, F. Barbier, J. Furtado, Inhibitory effect of oxygen on hydrogen-induced fracture of A333 pipe steel, Fatigue and Fracture of Engineering Materials and Structures 42 (2019) 1387–1401.
- [72] B. Somerday, P. Sofronis, K. Nibur, C. San Marchi, R. Kirchheim, Elucidating the variables affecting accelerated fatigue crack growth of steels in hydrogen gas with low oxygen concentrations, Acta Materialia 61 (2013) 6153–6170. doi:10.1016/j.actamat.2013.07.001.
- [73] J. Ronevich, C. San Marchi, R. Kolasinski, K. Thurmer, N. Bartelt, F. El Gabaly, B. Somerday, Oxygen impurity effects on hydrogen assisted fatigue and fracture of x100 pipeline steel 6B: Materials and Fabrication (2018) V06BT06A027. doi:10.1115/PVP2018-84163.
- [74] Z. Nan, R. Komoda, K. Yamada, C. Volkert, L. Tian, R. Kirchheim, P. Sofronis, H. Zahra, M. Dadfarnia, M. Kubota, A. Staykov, Effect of ammonia impurity on hydrogen embrittlement of SCM440 low-alloy steel in hydrogen gas, Proceedings of the Thirtieth International Ocean and Polar Engineering Conference (2020) 3030–3035.
- [75] V. Srikrishnan, P. Ficalora, Role of gaseous impurities in the hydrogen embrittlement of steel, Journal of Vacuum Science and Technology 14 (1977) 588–592. doi:10.1016/j.jhydene.2023.06.198.